Effect of residual many-body forces due to the evolution in the in-medium similarity renormalization group method.

G. Puddu

Dipartimento di Fisica dell'Universita' di Milano,

Via Celoria 16, I-20133 Milano, Italy

March 21, 2019

Abstract

In the past few years in-medium similarity renormalization group methods have been introduced and developed. In these methods the Hamiltonian is evolved using a unitary transformation in order to decouple a reference state from the rest of the Hilbert space. The evolution by itself will generate, even if we start from a two-body interaction, many-body forces which are usually neglected. In this work we estimate the effect of these residual many-body forces by comparing results obtained with the Hybrid Multi-determinant method, which keeps the Hamiltonian within the two-body sector, with the corresponding ones obtained with the in-medium similarity renormalization group. Although percentage-wise the effect of neglecting these induced many-body forces is not too large, they can be appreciable

1

depending on the nucleus, the shell model space and the harmonic oscillator frequency.

1   Introduction.

In the past years we have witnessed the development of powerful ab-initio many-body techniques to solve the nuclear Schroedinger equation. Among these methods we mention the no-core shell model (NCSM) (refs. [1]-[4]), the coupled-cluster method (refs.[5]-[8]) and the in-medium similarity renormalization group (IM-SRG) (see refs.[9],[10] for comprehensive reviews and references in there). As well known the limitation of the NCSM is the size of the Hilbert space. However, where applicable, the NCSM gives exact results. In the IM-SRG approach the many-body Hamiltonian is transformed with a unitary many-body operator. The discussion that follows is applied only to two-body forces and we shall consider only closed shell nuclei.

The key idea of the IM-SRG is as follows. The original Hamiltonian is first rewritten in normal form with respect to a reference state. In order to achieve this the formalism of Kutzelnigg and Mukherjee (ref.[11]) is used by which the original Hamiltonian, written with the particle vacuum as a reference state, is rewritten with a different reference state as a vacuum. For closed shell nuclei, the simplest choice is to use a single Slater determinant as a reference state, usually the spherical Hartree-Fock solution. The Hamiltonian acquires a zero-body term, a normally ordered one-body term and the normally ordered two-body interaction. The next step is the definition of a unitary operator which transforms this new Hamiltonian into a Hamiltonian such that the reference state is decoupled from the rest of the Hilbert space. This is achieved via a flow equation. There are several choices for this unitary operator (cf. refs.[9],[10]). This parameter-dependent flow equation will give, at the end, the ground-state energy as the the zero-body coefficient. Effectively the flow will transform the original Hamiltonian into a

block diagonal form with the ground-state decoupled from the rest of the Hilbert space. As well known, the flow will also generate induced many-body interactions which are normally neglected (this is the so-called IM-SRG(2) truncation). Hence, although we started with a two-body interaction only, the exact flow is approximated at the IM-SRG(2) level discarding all induced many-body interactions. It is natural to address the question about the accuracy of this truncation. Ideally we would like to compare IM-SRG(2) (which will call simply IM-SRG from now on) results with methods that do not generate induced many-body forces. An ideal method would be to compare the IM-SRG results with the shell model diagonalization in the full Hilbert space using Lanczos methods. However this can be done for light nuclei and not too large single-particle spaces. Here we use the Hybrid Multi-Determinant method (HMD)(refs.[12],[13]) complemented by energy versus variance of energy extrapolation techniques (EVE) (refs.[14]-[20]). Although computationally more demanding than the IM-SRG, it does not generate induced many-body forces, and in principle its applicability does not depend on the size of the Hilbert space. The key idea of the HMD method is to expand the nuclear wave function as a linear combination of many generic Slater determinants (with exact or approximate restoration of good quantum numbers using projectors) and to determine these Slater determinants using energy minimization techniques. The final EVE step consists in the evaluation of the energy variance (or related quantities) $< (\hat{H} - < \hat{H} >)^2 >$, $\hat{H}$ being the two-body Hamiltonian, once a set of approximate wave functions has been determined. The energy has a linear or linear+quadratic behavior as a function of the above variance. Extrapolation to zero variance will give the ground state energy. Although applicable, the HMD method becomes more and more computationally intensive as we increase

4

the single-particle space. Therefore we consider, in this work, Hamiltonians generated from the bare Hamiltonian for the nucleus of interest by the Lee-Suzuki (LS) renormalization technique (refs.[21]-[24]). Alternatively one could evolve first the two-body interaction with the similarity renormalization group in the vacuum, in order to soften the two-body interaction (refs.[25]-[28]). This preliminary step defines the Hamiltonian in the two-body sector which we use to perform the comparison.

The outline of this paper is as follows. In section 2 we briefly discuss the Hamiltonian we consider. In section 3 we recall briefly the HMD method, in section 4 we outline the spherical IM-SRG flow equations (see also ref.[10]) using the Brillouin generator (ref.[9]). In section 5 we compare the results in an harmonic oscillator basis for ^{4}He and for ^{16}O, and in section 6 we give some conclusions.

2   The Hamiltonian.

We start from the two-body Hamiltonian

$$\hat{H} = \sum_{i=1}^{A} \frac{p_i^2}{2m} + \sum_{i<j} V_{ij} \tag{1}$$

where m is the nucleon mass and V_{ij} is the interaction between nucleons i and j. Here we consider the chiral $N3LO$ interaction of Entem and Machleidt (ref.[29]). Much in the same way it is done in the NCSM (ref. [2]) we add a confining harmonic oscillator potential for the center of mass and obtain an A-dependent Hamiltonian. If ω is the frequency of this potential, the Hamiltonian can be recast in the following form

$$\hat{H}_\omega = \hat{H} + \frac{1}{2}mA\omega^2 R_{c.m.}^2 = \sum_{i=1}^{A} h_i + \sum_{i<j} V_{ij}^{(A)} \tag{2}$$

with

$$V_{ij}^{(A)} = V_{ij} - \frac{m\omega^2}{2A}(\vec{r}_i - \vec{r}_j)^2 \tag{3}$$

and

$$h_i = \frac{p_i^2}{2m} + \frac{1}{2}m\omega^2 r_i^2 \tag{4}$$

At the level of the 2-cluster approximation (ref.[2]), the 2-particle Hamiltonian which is the input of the LS method, is the intrinsic part of

$$\hat{H}_{12} = h_1 + h_2 + V_{12}^{(A)} = h_{rel} + h_{cm} \tag{5}$$

The intrinsic A-dependent two-particle Hamiltonian h_{rel} in eq.(5) is renormalized. First all matrix elements of h_{rel} are evaluated in the center of mass frame using no less than 200 major shells. The radial integrals were evaluated using 3000 integration points. We then renormalize this Hamiltonian using, as the P space, all relative-momentum HO states having pair quantum numbers n, l satisfying $2n + l \leq 2N_{lab}$. The Q space is comprised of all HO states not included in the P space. For numerical stability we use the method due to Kvaal (ref.[30]).

We augment the degrees of freedom by including the center of mass degrees of freedom and then translate this Hamiltonian to the lab frame using the Talmi-Moshinski brackets (cf. ref. [31] for a numerically efficient method and available subroutines). The single-particle space in the lab frame is limited to $2n+l \leq N_{lab}$. We consider here only an harmonic oscillator basis. For the details of the implementation see ref. [32] (especially the appendix). In principle, if carried out exactly, the renormalization prescription should generate multiparticle effective potentials. We discard all induced many-body interactions and define our model Hamiltonian solely in the two-body sector. We do not pretend that this Hamiltonian to accurately describe the nucleus under consideration, we simply stress that

we use the above prescription as a definition of the two-body Hamiltonian for the nucleus. This Hamiltonian may or may not include the harmonic oscillator center of mass term $\beta(\hat{H}_{cm} - 3\hbar\omega/2)$. In order to simplify as much as possible the comparison with the IM-SRG method we consider N_{lab} as low as possible. Although large N_{lab} values can be handled by the IM-SRG method, it would be problematic to compare IM-SRG results with those which work strictly within the two-body sector, since we wish to assess the importance of the many-body forces omitted in the IM-SRG flow.

3   A brief recap of the HMD method.

The Hybrid-Multi-Determinant (HMD) method consists in generating more and more accurate wave-functions with linear combinations of many particle-number conserving Slater determinants which are determined with quasi-Newtonian energy minimization techniques (cf. ref. [33]). We use a rank-3 update technique described in details in ref.[34]. The wave-function of the nucleus is written as

$$|\psi> = \sum_{S=1}^{N_D} g_S \hat{P}|U_S> \tag{6}$$

where $\hat{P}$ is a projector to good quantum numbers (e.g. good angular momentum and parity) N_D is the number of Slater determinants $|U_S>$ expressed as

$$|U_S> = \overline{c}_1(S)\overline{c}_2(S)...\overline{c}_A(S)|0> . \tag{7}$$

The generalized creation operators $\overline{c}_\alpha(S)$ for $\alpha = 1, 2, .., A$ are a linear combination of the creation operators $a_i^\dagger$

$$\overline{c}_\alpha(S) = \sum_{i=1}^{N_s} U_{i,\alpha}(S)a_i^\dagger \quad \alpha = 1, ...A \tag{8}$$

Here N_s is the number of the single-particle states. The complex coefficients $U_{i,\alpha}(S)$ represent the single-particle wave-function of the particle $\alpha = 1, 2, .., A$. We do not impose any symmetry on the Slater determinants (axial or other) since the $U_{i,\alpha}$ are variational parameters. These complex coefficients are obtained by minimizing the energy expectation values

$$E[U] = \frac{< \psi|\hat{H}|\psi >}{< \psi|\psi >} \tag{9}$$

The coefficients g_S are obtained by solving the generalized eigenvalue problem

$$\sum_S < U_{S'}|\hat{P}\hat{H}|U_S > g_S = E \sum_S < U_{S'}|\hat{P}|U_S > g_S \tag{10}$$

for the lowest eigenvalue E. We normally consider projectors to good $z-$ component of the angular momentum and parity, rather than projectors to good angular momentum and parity. The number of Slater determinants necessary for convergence can be quite large. Hence as a final step we use EVE techniques (we implement the variant of ref.[19]). These techniques consist in the evaluation of the energy variance

$$\sigma^2 = < \hat{H}^2 > - < \hat{H} >^2 \tag{11}$$

as a function of the energy $< \hat{H} >$. On general grounds $< \hat{H} >$ is a linear or linear+quadratic function of σ^2 provided we are sufficiently close to the ground-state (here we are primarily concerned about ground-state energies). The clause "sufficiently close" is basic. In fact, we extrapolate the plot $< \hat{H} >$ as a function of σ^2 to $\sigma^2 = 0$. Even small uncertainties in the coefficients of the expansion can cause sizable error in the extrapolated ground-state energies if we are not sufficiently close to $\sigma^2 = 0$. Differently stated, the linear+quadratic fit must be of high quality. In practice, we generated a few hundreds Slater determinants as sketched above, we then evaluate σ^2 and $< \hat{H} >$ for a partial linear combination until we

8

include them all. As a final step we employ the linearization method introduced in ref. [18] to optimize the order of the Slater determinants, More precisely, we construct a set of point $(\sigma^2, <\hat{H}>)$ using wave-functions $|\psi> = \sum_{S=1}^{N} g_S \hat{P} |U_S>$ for all $N \leq N_D$ after these Slater determinants have been reordered so that the points $(\sigma^2, <\hat{H}>)$ can be fitted with a linear+quadratic curve.

4   A brief description of the IM-SRG method.

Self-contained and detailed descriptions of the IM-SRG method and its applications can be found in the review papers of refs. [9],[10]. Here we simply describe how it has been implemented in this work. The basic idea is to evolve the many-body Hamiltonian with a continuous set of unitary operators $\hat{U}(s)$

$$\hat{H}(s) = \hat{U}(s)\hat{H}\hat{U}(s)^{\dagger} \tag{12}$$

The flow equation is then given by

$$\frac{d\hat{H}(s)}{ds} = [\hat{\eta}(s), \hat{H}(s)] \tag{13}$$

where the generator $\hat{\eta}(s)$ is given by $\hat{\eta}(s) = \frac{d\hat{U}(s)}{ds}\hat{U}(s)^{\dagger}$. An approximate ground-state wave-function $|\phi>$ is selected and the initial Hamiltonian is rewritten in normal form with respect to $|\phi>$ as a vacuum. Both the generator and the evolved Hamiltonian are truncated at the two-body level as

$$\hat{\eta}(s) = \sum_{ij} \eta_j^i(s) : \hat{A}_j^i : + (1/4) \sum_{ijkl} \eta_{kl}^{ij}(s) : \hat{A}_{kl}^{ij} : \tag{14}$$

$$\hat{H}(s) = E(s) + \sum_{ij} f_j^i(s) : \hat{A}_j^i : + (1/4) \sum_{ijkl} \Gamma_{kl}^{ij}(s) : \hat{A}_{kl}^{ij} : \tag{15}$$

Here we use the tensor notation commonly employed in the IM-SRG method, that is $\hat{A}_j^i = a_i^\dagger a_j$ and $\hat{A}_{kl}^{ij} = a_i^\dagger a_j^\dagger a_l a_k$. As usual, the colons denote normal ordering to the reference state $|\phi>$. We use the Brillouin generator since $\frac{dE(s)}{ds}$ assumes a particularly appealing form. Since we study only closed shell systems we use a single reference $|\phi>$, as usually done for closed (sub)shells. In order to save computer memory we work in the angular momentum coupled representation. We solve the flow equations $\frac{dE(s)}{ds}$, $\frac{df(s)}{ds}$ and $\frac{d\Gamma(s)}{ds}$ using the Runge-Kutta method of rank 3 (cf. ref.[35])) with $\Delta s = 0.000025$ until the energy no longer changes. The relevant flow equations in the coupled representations are described in the Appendix, using as a basis the natural orbit representation that diagonalized the expectation values of the one-body density. Three-body and higher rank terms arise from the commutator in eq.(13) and they are unavoidable in this method. In principle these depend of the choice of the reference state. As discussed in the next section, we in particular want to study the eventual discrepancy between the HMD method in which the whole Hamiltonian remains in the two-body sector and the IM-SRG results. We expect a dependence on the reference state, on the harmonic oscillator frequency $\hbar\omega$ and on the size of the single particle space defined by N_{lab}. We will use two single-reference states. The spherical Hartree-Fock solution and a naive filling of the lower harmonic oscillator orbits. Note that in section 5 of ref.[10] for ^4He a discrepancy between IM-SRG binding energy and the one obtained with the Fadeev-Jakubowski method has already been found a bit large, pointing out to a sizable effect of the neglected induced many-body forces in the evolution. Presumably these discrepancies can be reduced using the more involved multi-reference states as done recently in ref.[36].

5 Numerical results.

We considered the cases of ^4He and ^{16}O. For ^4He we considered the following cases. The harmonic oscillator frequencies (in MeV's) are $\hbar\omega = 24, \quad 38$ for $N_{lab} = 3, 4, 5$. For ^{16}O, $\hbar\omega = 14$ with $N_{lab} = 3, 4, 5$, for $\hbar\omega = 24$ $N_{lab} = 2, 3, 4$ and for $\hbar\omega = 32$ with $N_{lab} = 2, 3$. It should be pointed out that changing N_{lab} the Hamiltonian changes. It does not correspond to a different truncation. Hence we do not expect a monotonic behavior of the energies as we increase N_{lab}. The largest size of the Hilbert space for $J_z^\pi = 0^+$ is about 10^{22} for ^{16}O with $N_{lab} = 5$, while for $N_{lab} = 3$ and $N_{lab} = 4$ the size of the Hilbert space is 4×10^{14} and 5×10^{18} respectively. For ^4He with $N_{lab} = 5$ the corresponding number is 3.529.304. In the ^{16}O cases we added to the Hamiltonian a center of mass term with $\beta = 1 MeV$. The results are summarized in the tables. Let us discuss first the ^4He. The HMD results for ^4He are rather accurate. An estimate of the uncertainty for $N_{lab} = 3, 4, 5$ is about a dozen KeV's. We considered two reference states for the IM-SRG calculations. One is the naive Fermi filling (FF) of the lowest single-particle states and the other is the spherical HF. Notice that for the lowest value of $\hbar\omega = 24 MeV$ the discrepancies between the various methods increases with N_{lab}. This discrepancy increases for the largest value of $\hbar\omega$. This discrepancy is substantial and is qualitatively in agreement with the findings of ref. [10] where the IM-SRG results for large single-particle spaces have been compared with the exact binding energy for this interaction. It is instructive to plot the results for $E(s)$ at large s obtained with the IM-SRG with the corresponding ones obtained with the HMD. In figs. (1)-(6) we show this comparison. For the ^4He cases, the uncertainties of the HMD method are best quantified by plotting $E(\sigma^2)$ vs. σ^2 together with the linear+quadratic fit. This is done in figs. (7)-(8) for $N_{lab} = 5$.

$\hbar\omega(MeV)$	N_{lab}	HMD	FF(MeV)	HF(MeV)
24	3	-25.798	-25.933	-25.932
	4	-24.670	-24.676	-24.975
	5	-24.127	-24.261	-24.888
38	3	-22.047	-21.145	-22.539
	4	-23.027	-21.989	-24.268
	5	-23.544	-22.264	-24.907

Table 1: Ground-state energies for ^4He obtained with the HMD method, with the IM-SRG with the Fermi filling (FF) and HF as a reference state. The experimental value is -28.295 MeV (ref.[37])

$\hbar\omega(MeV)$	N_{lab}	HMD	FF(MeV)	HF(MeV)
14	3	-149.634	-153.646	-148.680
	4	-139.826	-142.858	-138.301
	5	-133.397	-135.467	-130.081
24	2	-139.706	-139.699	-139.704
	3	-113.057	-110.416	-111.424
	4	-97.855	-93.243	-95.664
32	2	-53.921	-54.138	-54.185
	3	-62.823	-58.461	-61.097

Table 2: Ground-state energies for ^{16}O obtained with the HMD method, with the IM-SRG with the Fermi filling (FF) and HF as a reference state. The experimental value is -127.619MeV (ref.[37])
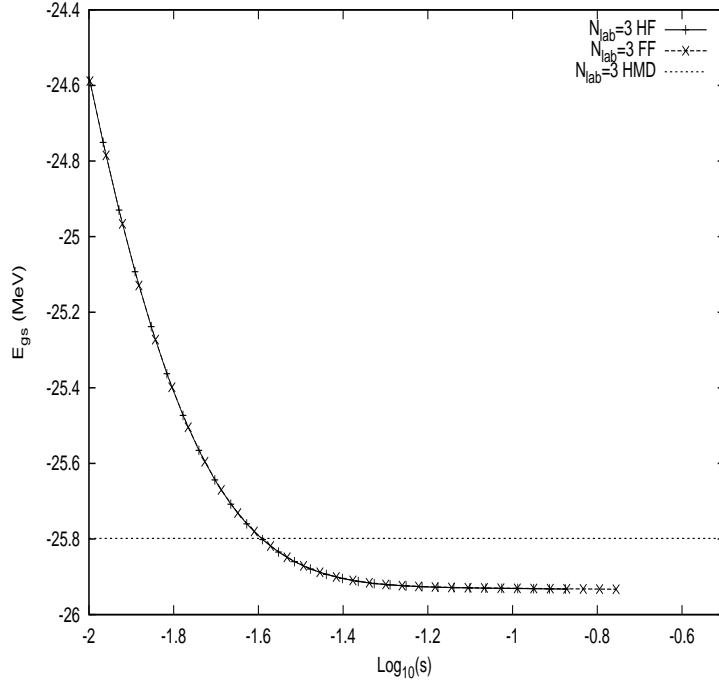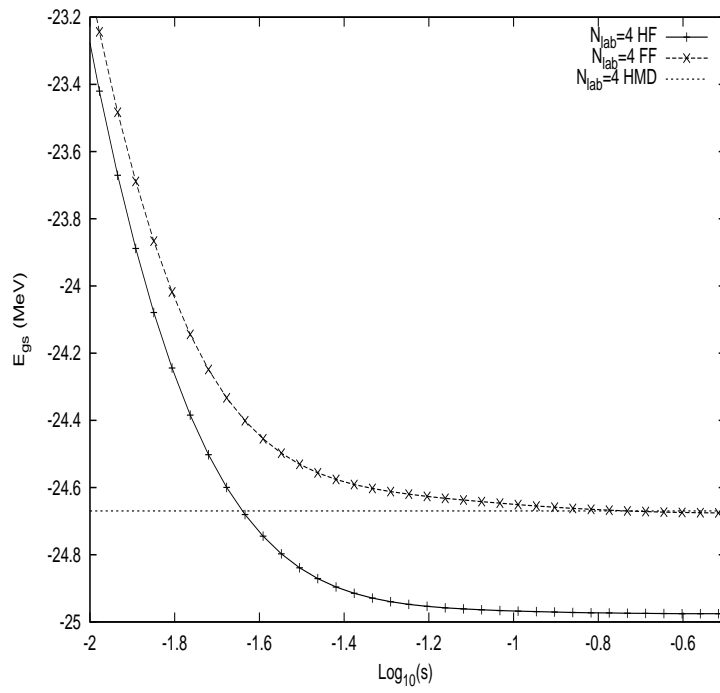
Figure 1: ^4He IM-SRG E(s)for large s for the two reference states discussed in the text, for $\hbar\omega = 24MeV$ and $N_{lab} = 3$. The horizontal line is the HMD result.

Notice that we considered only the end part (i.e. the one closer to the vertical axis) of the data points. The data points are close to the energy axis, and in such cases the extrapolated values are accurate. The case of ^{16}O is less certain. In principle we can get close to the energy axis in the EVE plot, but we would have to consider a large number of Slater determinants. In these cases we can estimate the uncertainty in the HMD method by performing several fits to different sets of $(\sigma^2, E(\sigma^2))$ data points. For some of the best fits the extrapolated values are shown in table 2.

In figs.(9)-(11) we plot the end part of the IM-SRG calculations for ^{16}O at $\hbar\omega = 14MeV$ and $N_{lab} = 3, 4, 5$ respectively together with the corresponding HMD results. The horizontal lines represent the HMD results. In some cases we

13

Figure 2: ^4He IM-SRG E(s)for large s for the two reference states discussed in the text, for $\hbar\omega = 24MeV$ and $N_{lab} = 4$. The horizontal line is the HMD result.
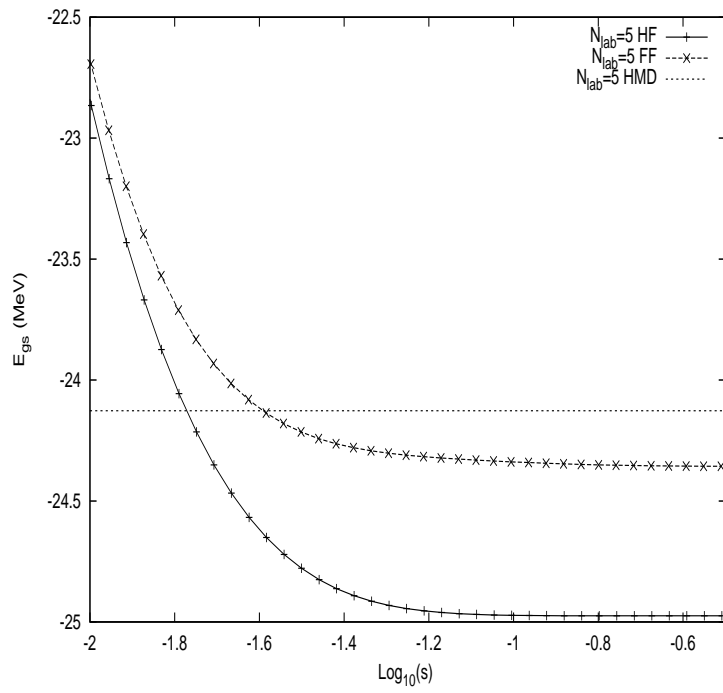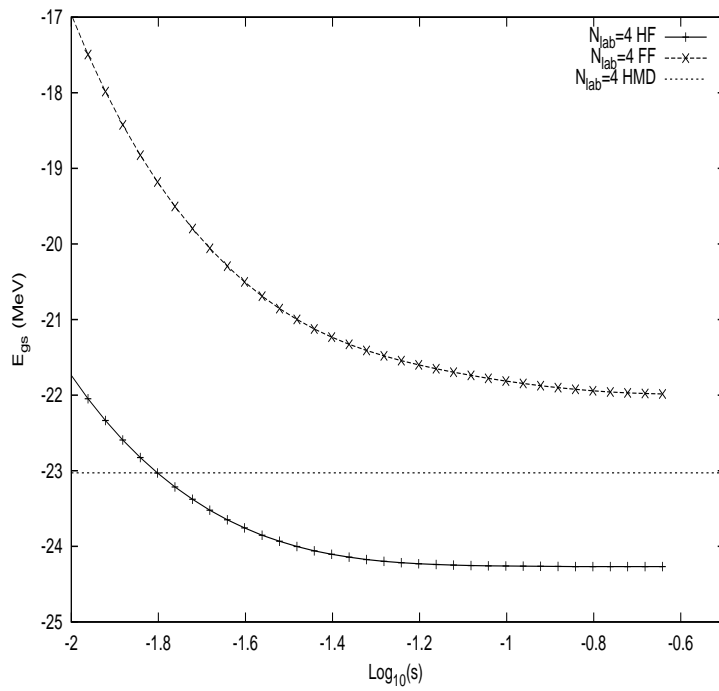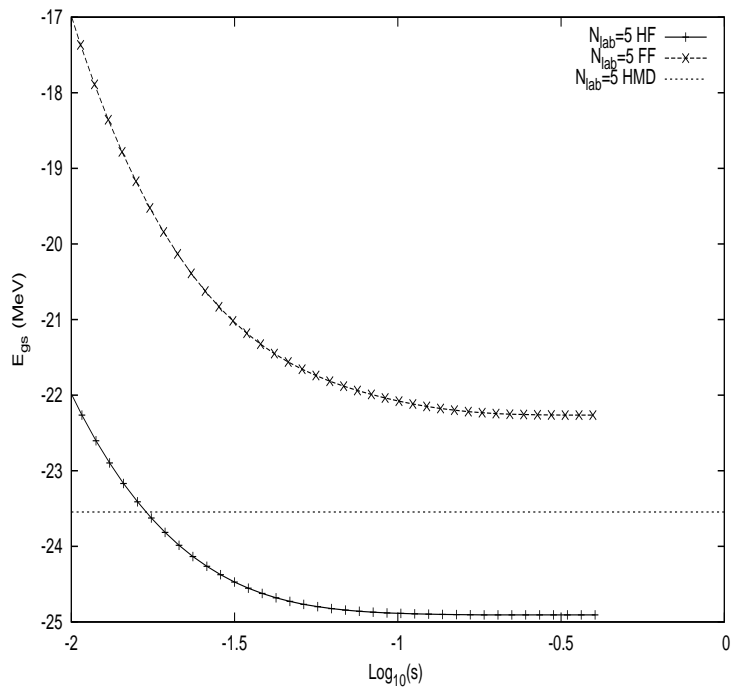
Figure 3: ^4He IM-SRG E(s)for large s for the two reference states discussed in the text, for $\hbar\omega = 24MeV$ and $N_{lab} = 5$. The horizontal line is the HMD result.

15
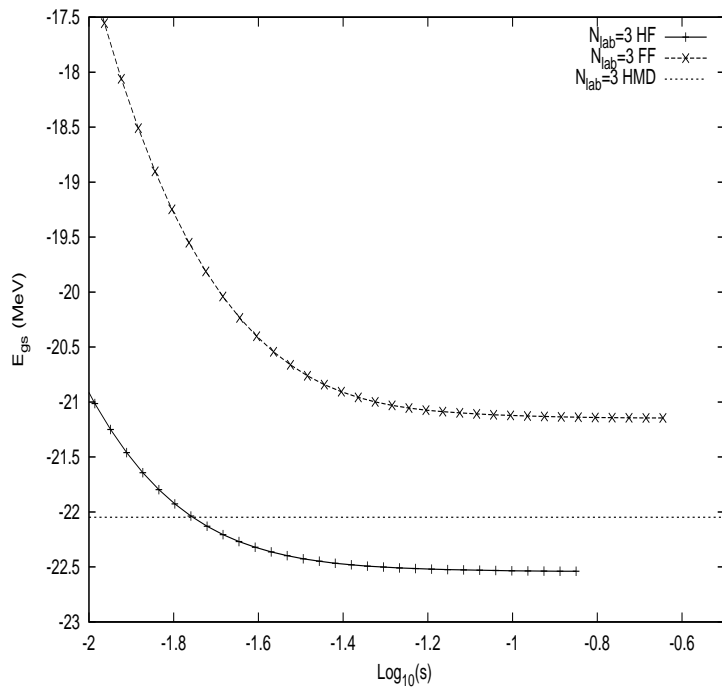
Figure 4: ^4He IM-SRG E(s)for large s for the two reference states discussed in the text, for $\hbar\omega = 38 MeV$ and $N_{lab} = 3$. The horizontal line is the HMD result.
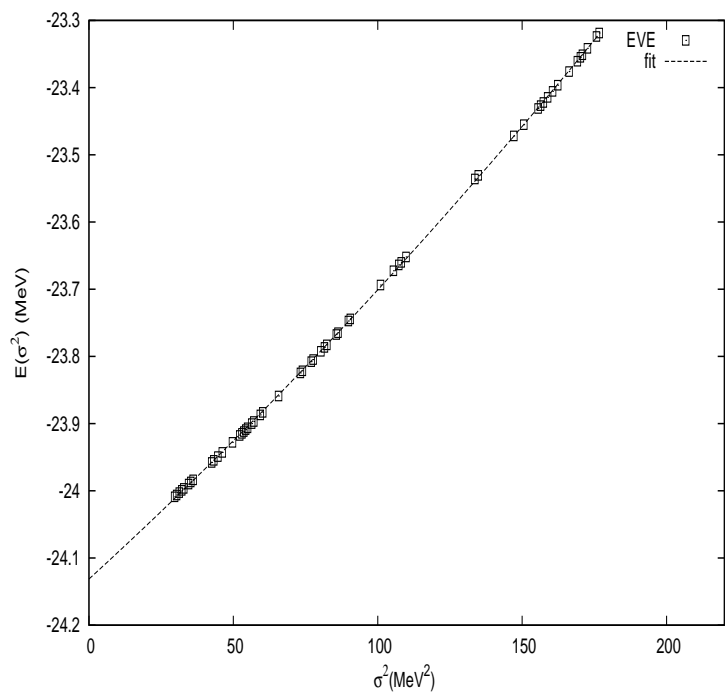
Figure 5: ^4He IM-SRG E(s)for large s for the two reference states discussed in the text, for $\hbar\omega = 38MeV$ and $N_{lab} = 4$. The horizontal line is the HMD result.

Figure 6: ^4He IM-SRG E(s)for large s for the two reference states discussed in the text, for $\hbar\omega = 38MeV$ and $N_{lab} = 5$. The horizontal line is the HMD result.

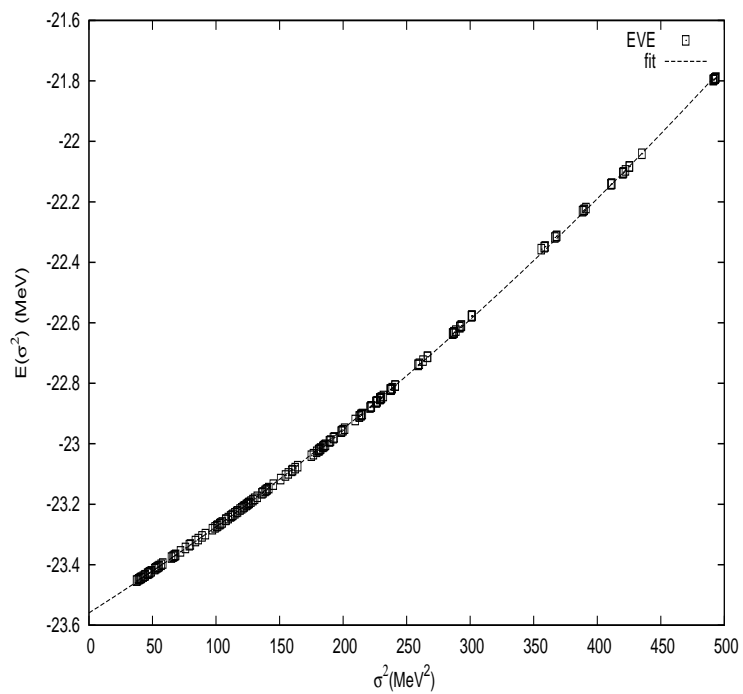Figure 7: EVE plot for ^4He for $\hbar\omega = 24 MeV$ and $N_{lab} = 5$.

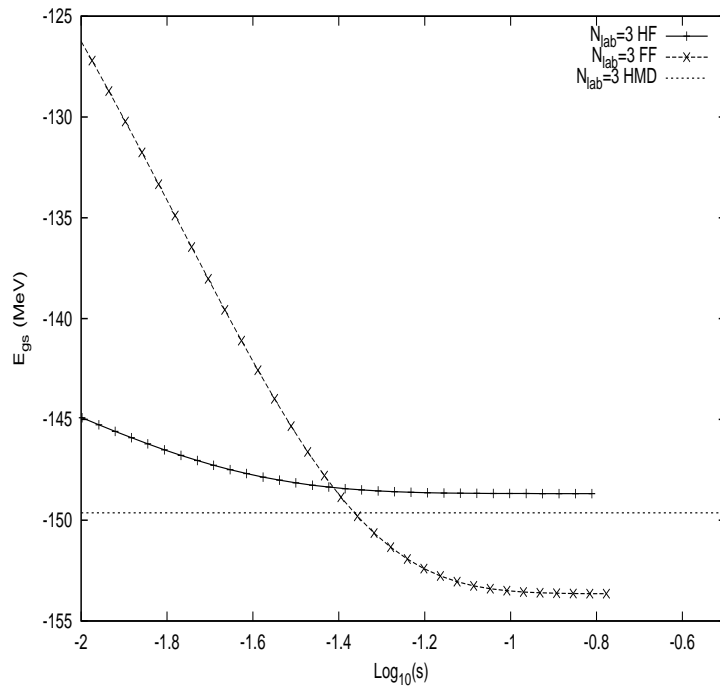Figure 8: EVE plot for ^4He for $\hbar\omega = 38MeV$ and $N_{lab} = 5$.

Figure 9: IM-SRG results for HF and FF(Fermi filling) for ^{16}O at $\hbar\omega = 14 MeV$ and $N_{lab} = 3$ together with the corresponding HMD results.
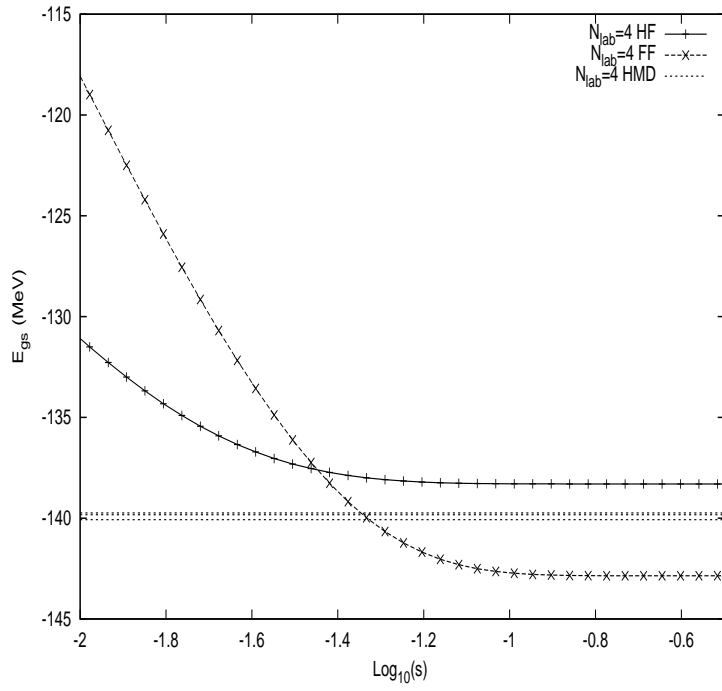
Figure 10: IM-SRG results for HF and FF(Fermi filling) for ^{16}O at $\hbar\omega = 14MeV$ and $N_{lab} = 4$ together with the corresponding HMD results.
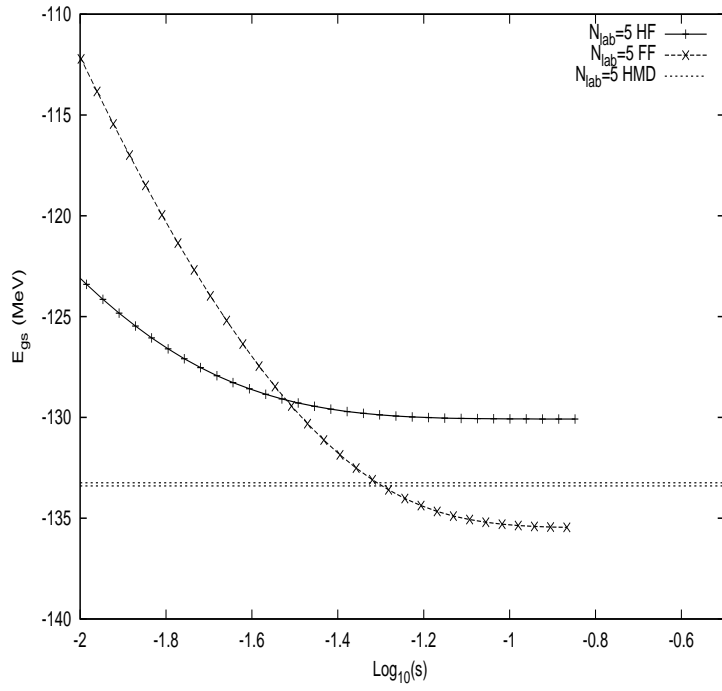
Figure 11: IM-SRG results for HF and FF(Fermi filling) for ^{16}O at $\hbar\omega = 14 MeV$ and $N_{lab} = 5$ together with the corresponding HMD results.
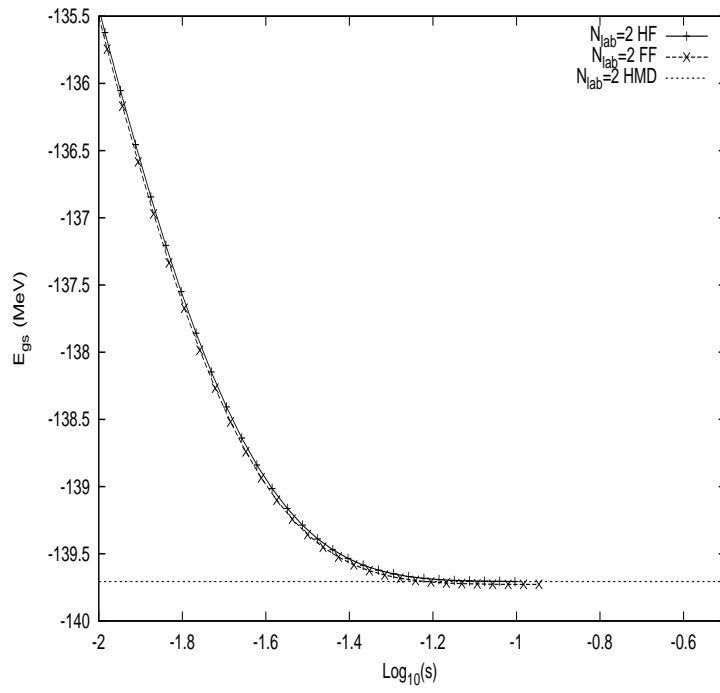
Figure 12: IM-SRG results for HF and FF(Fermi filling) for ^{16}O at $\hbar\omega = 24 MeV$ and $N_{lab} = 2$ together with the corresponding HMD results.
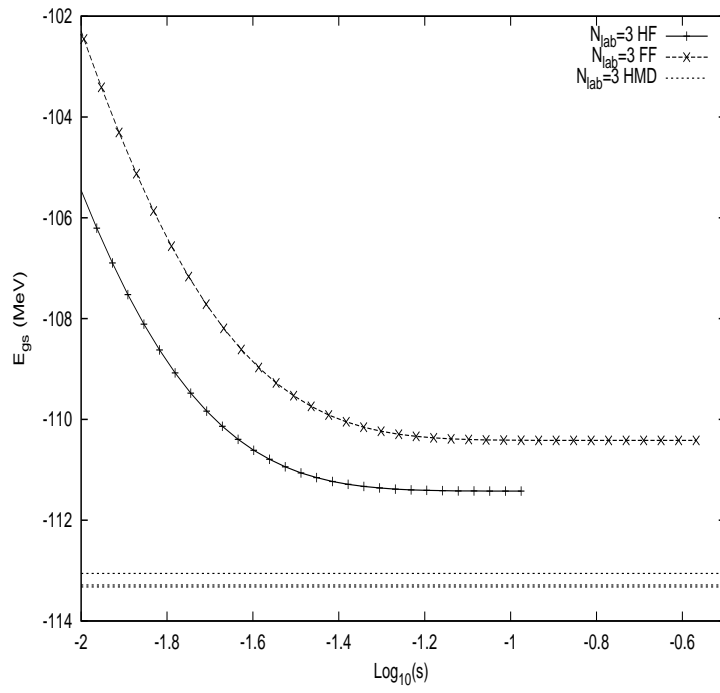
Figure 13: IM-SRG results for HF and FF(Fermi filling) for ^{16}O at $\hbar\omega = 24 MeV$ and $N_{lab} = 3$ together with the corresponding HMD results.

Figure 14: IM-SRG results for HF and FF(Fermi filling) for ^{16}O at $\hbar\omega = 24MeV$ and $N_{lab} = 4$ together with the corresponding HMD results.

Figure 15: IM-SRG results for HF and FF(Fermi filling) for ^{16}O at $\hbar\omega = 32MeV$ and $N_{lab} = 2$ together with the corresponding HMD results.

Figure 16: IM-SRG results for HF and FF(Fermi filling) for ^{16}O at $\hbar\omega = 32MeV$ and $N_{lab} = 3$ together with the corresponding HMD results.
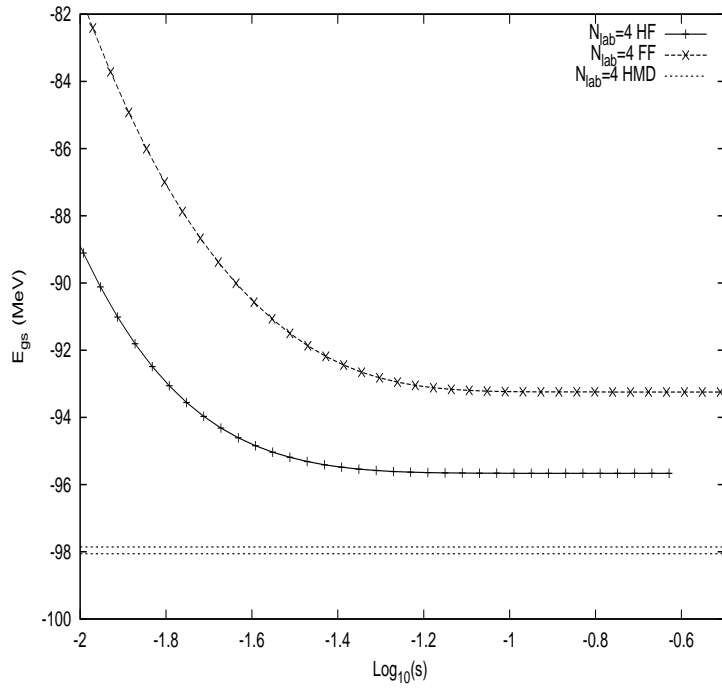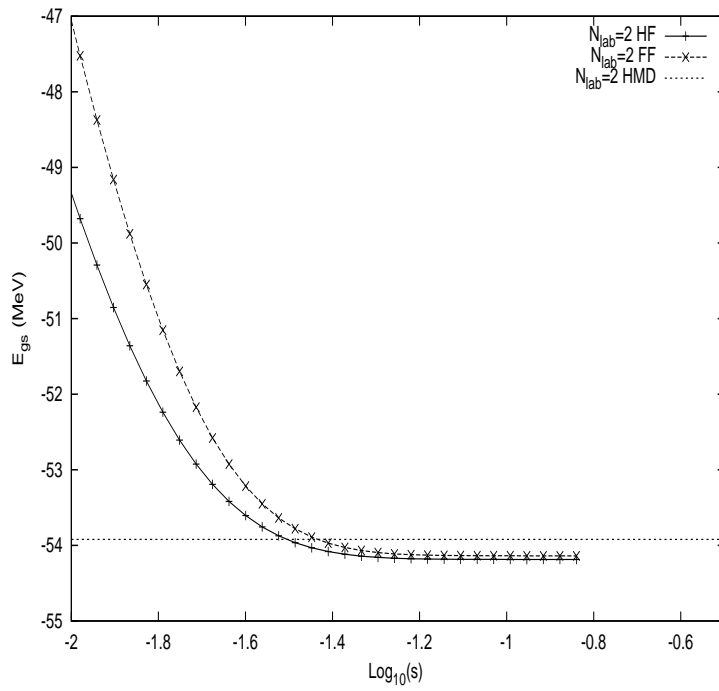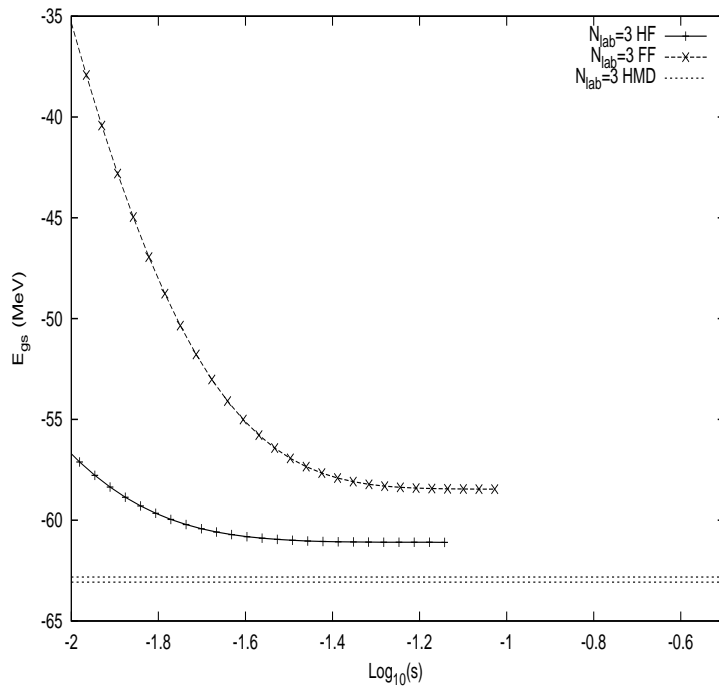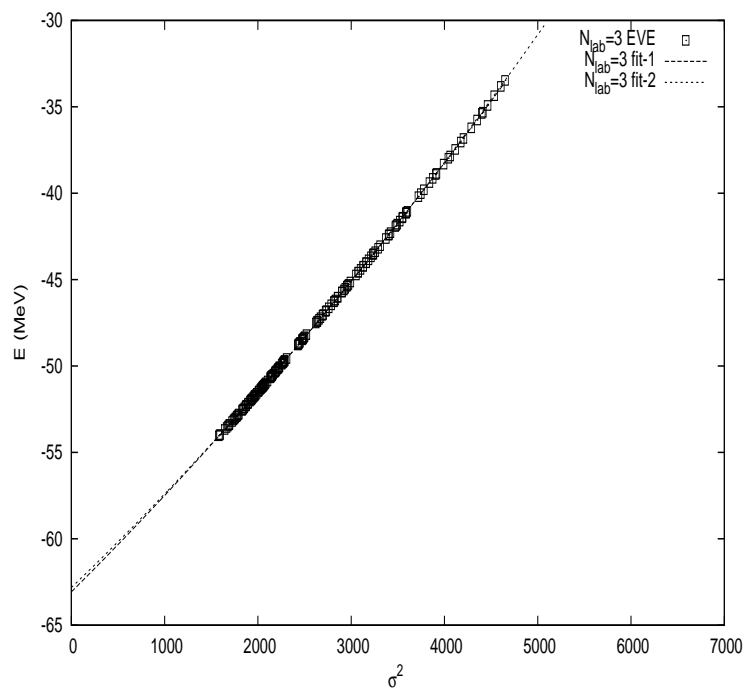
Figure 17: EVE results for ^{16}O, $\hbar\omega = 32MeV$ and $N_{lab} = 3$.

display different fits. In figs.(12)-(14) we display the results for $\hbar\omega = 24 MeV$ and $N_{lab} = 2, 3, 4$, and in figs.(15)-(16) the results for $\hbar\omega = 32 MeV$ and $N_{lab} = 2, 3$. Notice, as in the case of ^4He, that discrepancies increase with $\hbar\omega$ and N_{lab}. The IM-SRG becomes more and more sensitive to the reference state. In order to judge the quality of the EVE extrapolation of the HMD calculations, in fig. (17) we show a typical EVE plot $(\sigma^2, E(\sigma^2)$ and two linear+quadratic fits for ^{16}O with $\hbar\omega = 32 MeV$ and $N_{lab} = 3$. Notice that the uncertainty of the fits is determined by the distance of the data from the energy axis. Needless to say by increasing the number of Slater determinants we decrease the energy and the variance and, as a consequence, the uncertainty. In all plots of the IM-SRG results we decimated the data points in order to avoid clutter. In the cases of the EVE extrapolations we select those linear+quadratic fits which have the the smallest average discrepancy from the actual calculations.

Before leaving this section, we stress that single-reference IM-SRG is usually applied only to closed shell nuclei. For open shell nuclei the more involved multi-reference version is preferred. the multi-reference IM-SRG version contains however all irreducible rank-2 and rank-3 densities (cf. refs.[9],[38] for more details). The importance-truncated NCSM (ref.[39]) can also be used to assess the net effect of the many-body forces induced by the IM-SRG flow. We limited ourselves to small single-particle spaces, since the comparison between single-reference IM-SRG results and exact or quasi-exact results is simple. Needless to say, for a comparison with experimental data much larger single-particle spaces are needed in order to soften the $\hbar\omega$ and N_{lab} dependence.

6 Conclusions.

In this work we have performed HMD with EVE extrapolation techniques in order to ascertain the overall contribution of the many-body forces induced by the IM-SRG evolution. They depend on the reference state, on the harmonic oscillator frequency and on the size of the single-particle space. Although percentage-wise these missing many-body forces give a contribution of the order of few per cent, their importance seems to increase for increasing harmonic oscillator frequency and with the size of the single-particle space. Most likely they become less relevant in the more general multi-reference IM-SRG.

7 Appendix.

We work in the representation that diagonalized the one-body density matrix, i.e. $< \hat{A}^i_j >= n_i \delta_{ij}$. We consider only real quantities. For completeness we also give the $M-$scheme flow equations (cf.ref.[9] for the more general case of multi-reference state and other generators), restricting ourselves to the Brillouin generator given by (we omit for simplicity the s dependence)

$$\eta^i_j = f^j_i(n_j - n_i) \qquad (A1)$$

$$\eta^{ij}_{kl} = \Gamma^{kl}_{ij}(n_k n_l \overline{n}_i \overline{n}_j - \overline{n}_k \overline{n}_l n_i n_j) \qquad (A2)$$

The gradients of the energy, of the one-body and of the two-body term are respectively

$$\frac{dE}{ds} = -\sum_{ab}(\eta^a_b)^2 - \frac{1}{4}\sum_{abcd}(\eta^{ab}_{cd})^2 \qquad (A3)$$

$$\frac{df^i_j}{ds} = \sum_a(\eta^i_a f^a_j - f^i_a \eta^a_j) + \sum_{ab}(n_a - n_b)(\eta^a_b \Gamma^{bi}_{aj} - f^a_b \eta^{bi}_{aj})$$

$$+\frac{1}{2}\sum_{abc}(n_a\overline{n}_b\overline{n}_c + \overline{n}_an_bn_c)(\eta_{bc}^{ia}\Gamma_{ja}^{bc} - \Gamma_{bc}^{ia}\eta_{ja}^{bc}) \qquad (A4)$$

$$\frac{d\Gamma_{kl}^{ij}}{ds} = \sum_a[(\eta_a^i\Gamma_{kl}^{aj} + \eta_a^j\Gamma_{kl}^{ia} - \eta_k^a\Gamma_{al}^{ij} - \eta_l^a\Gamma_{ka}^{ij})$$

$$-(f_a^i\eta_{kl}^{aj} + f_a^j\eta_{kl}^{ia} - f_k^a\eta_{al}^{ij} - f_l^a\eta_{ka}^{ij})]$$

$$+\frac{1}{2}\sum_{ab}(1 - n_a - n_b)(\eta_{ab}^{ij}\Gamma_{kl}^{ab} - \Gamma_{ab}^{ij}\eta_{kl}^{ab})$$

$$+\sum_{ab}(n_a - n_b)[(\eta_{kb}^{ia}\Gamma_{la}^{jb} - \Gamma_{kb}^{ia}\eta_{la}^{jb}) - (\eta_{kb}^{ja}\Gamma_{la}^{ib} - \Gamma_{kb}^{ja}\eta_{la}^{ib})] \qquad (A5)$$

In the above equations all single-particle indices comprise the m quantum numbers and $\overline{n} = 1 - n$. The last term in eq.(A5) is referred to as the cross-term, and it is the most troublesome in going to the angular momentum coupled representation. The variational character of the Brillouin generator is apparent in this form of the energy gradient.

In the coupled representation (the $J-$flow) and for closed shells the single-particle labels comprise the radial, the angular momentum and the isospin quantum numbers only, e.g. $i = (k_i, l_i, j_i, \tau_i)$. All one-body quantities are diagonal in the l, j, τ quantum numbers. The Brillouin generators become

$$\eta_j^i = f_i^j(n_j - n_i) \qquad (A6)$$

$$\eta_{kl}^{ij}(J) = \Gamma_{ij}^{kl}(J)(n_kn_l\overline{n}_i\overline{n}_j - \overline{n}_k\overline{n}_ln_in_j) \qquad (A7)$$

for the one-body and two-body parts respectively. J is the total two-body angular momentum in which two-body matrix elements are diagonal and M independent. We use the notation $\hat{j} = \sqrt{2j + 1}$. The energy gradient $\frac{dE}{ds}$ is given by

$$\frac{dE}{ds} = -\sum_{ab}\delta_{j_a,j_b}\delta_{l_a,l_b}\delta_{\tau_a,\tau_b}\hat{j}_a^2(\eta_b^a)^2 - \frac{1}{4}\sum_{abcdJ}\hat{J}^2[\eta_{cd}^{ab}(J)]^2 \qquad (A8)$$

The δ's are Kronecker deltas. The gradient of the one-body term is given by

$$\frac{df_j^i}{ds} = \sum_a\delta_{j_i,j_a}(\eta_a^if_j^a - f_a^i\eta_j^a) + \frac{1}{\hat{j}_i^2}\sum_{abJ}\hat{J}^2(n_a - n_b)[\eta_b^a\Gamma_{aj}^{bi}(J) - f_b^a\eta_{aj}^{bi}(J)]$$

$$+\frac{1}{2\hat{j}_i^2}\sum_{abcJ}\hat{J}^2(n_a\overline{n}_b\overline{n}_c + \overline{n}_a n_b n_c)[\eta_{bc}^{ia}(J)\Gamma_{ja}^{bc}(J) - \Gamma_{bc}^{ia}(J)\eta_{ja}^{bc}(J)] \qquad (A9)$$

The flow equation for Γ is more involved. For readability, we separate contributions to the gradient of Γ in three terms

$$\frac{d\Gamma_{kl}^{ij}(J)}{ds} = C_{kl}^{ij}(J) + D_{kl}^{ij}(J) + E_{kl}^{ij}(J) \qquad (A10)$$

where

$$C_{kl}^{ij}(J) = \sum_a \{[\eta_a^i\Gamma_{kl}^{aj}(J) - f_a^i\eta_{kl}^{aj}(J)] + [\eta_a^j\Gamma_{kl}^{ia}(J) - f_a^j\eta_{kl}^{ia}(J)] -$$

$$[\eta_k^a\Gamma_{al}^{ij}(J) - f_k^a\eta_{al}^{ij}(J)] - [\eta_l^a\Gamma_{ka}^{ij}(J) - f_l^a\eta_{ka}^{ij}(J)]\} \qquad (A11)$$

and

$$D_{kl}^{ij}(J) = \frac{1}{2}\sum_{ab}(1 - n_a - n_b)[\eta_{ab}^{ij}(J)\Gamma_{ij}^{ab}(J) - \Gamma_{ab}^{ij}(J)\eta_{ij}^{ab}(J)] \qquad (A12)$$

The cross-coupled term E is more involved. Define first

$$W_{kl}^{ij}(J) = (-1)^{J+j_j+j_l}\sum_{ab}(n_a - n_b)\sum_K \hat{K}^2\begin{Bmatrix} j_i & j_j & J \\ j_l & j_k & K \end{Bmatrix} \times$$

$$[\tilde{\eta}_K(k\overline{i}, b\overline{a})\tilde{\Gamma}_K(l\overline{j}, a\overline{b}) - \tilde{\Gamma}_K(k\overline{i}, b\overline{a})\tilde{\eta}_K(l\overline{j}, a\overline{b})] \qquad (A13)$$

where the tilde matrices are defined as

$$\tilde{O}_K(l\overline{j}, a\overline{b}) = \sum_J(-1)^J\hat{J}^2 O_{la}^{jb}(J)\begin{Bmatrix} j_j & j_l & K \\ j_a & j_b & J \end{Bmatrix} \qquad (A14)$$

The last contribution to $d\Gamma_{kl}^{ij}(J)/ds$ is then given by

$$E_{kl}^{ij}(J) = W_{kl}^{ij}(J) - (-1)^{j_i+j_j+J}W_{kl}^{ji}(J) \qquad (A15)$$

Apart a phase factor, the tilde operators are the Pandya transform of the corresponding ones without the tilde.

References

[1] P.Navratil, J.P.Vary and B.R.Barrett. Phys. Rev. Lett. 84 (2000)5728.

[2] P.Navratil, J.P.Vary and B.R.Barrett. Phys. Rev. C 62 (2000) 054311.

[3] P.Navratil, S.Quaglioni, I.Stetcu and B.R.Barrett.
J. Phys. G: Nucl. Part. Phys. 36 (2009)083101.

[4] B.R.Barrett, P.Navratil and J.P.Vary. Prog. Part. Nucl.
Phys. 69 (2013)131.

[5] M.Wloch, D.Dean, J.R.Gour, M.Hjorth-Jensen, K.Kowalski, T.Papenbrock,
and P.Piecuch, Phys. Rev. Lett. 94, 212501 (2005).

[6] G.Hagen, T.Papenbrock, D.J.Dean, and M.Hjorth-Jensen, Phys. Rev. Lett.
101, 092502 (2008).

[7] G. Hagen, M. Hjorth-Jensen, G. R. Jansen, R. Machleidt, and
T. Papenbrock, Phys. Rev. Lett. 109, 032502 (2012).

[8] G. Hagen, T. Papenbrock, D. J. Dean, and M. Hjorth-Jensen.
Phys. Rev. C 82,(2010) 034330

[9] H. Hergert. Phys. Scr. 92,023002(2017).

[10] H. Hergert, S.K. Bogner, T.D. Morris, A. Schwenk,
K. Tsukiyama. Physics Reports 621 (2016) 165.

[11] Kutzelnigg W and Mukherjee D. J. Chem. Phys. 107, 432(1997).

[12] G.Puddu. J. Phys. G: Nucl. Part. Phys. 44 105104(2017)

[13] G.Puddu J. Phys. G: Nucl. Part. Phys. 32 (2006) 321.

G.Puddu. Eur. Phys. J. A 31 (2), pp. 163 (2007).

G.Puddu. Eur. Phys. J. A 45, 233(2010).

[14] M. Imada and T. Kashima, J. Phys. Soc. Jpn. 69 2723 (2000).

[15] T. Mizusaki and M. Imada, Phys. Rev. C 65, 064319 (2002).

[16] T. Mizusaki and N. Shimizu, Phys. Rev. C 85, 021301(R)(2012).

[17] T. Mizusaki, Phys. Rev. C 70, 044316 (2004).

[18] N. Shimizu, Y. Utsuno, T. Mizusaki, T. Otsuka, T. Abe, and M. Honma, Phys. Rev. C 82, 061305(R) (2010).

[19] G.Puddu J. Phys. G: Nucl. Part. Phys. 39, 085108(2012).

[20] N.Shimizu, Y.Utsuno, T.Mizusaki, M.Honma, Y.Tsunoda and T.Otsuka Phys. Rev. C 85, 054301 (2012)

[21] 7. K. Suzuki, S.Y. Lee, Prog. Theor. Phys. 64, 2091 (1980).

[22] 8. K. Suzuki, Prog. Theor. Phys. 68, 1627 (1982).

[23] K. Suzuki, Prog. Theor. Phys. 68, 1999 (1982).

[24] K. Suzuki, R. Okamoto, Prog. Theor. Phys. 92, 1045 (1992).

[25] Bogner S K, Kuo T T S and Schwenk A. Phys. Rep. 386,1 (2003).

[26] Bogner S K, Furnstahl R J and Perry R J. Phys. Rev. C 75 061001(2007)

[27] Bogner S K, Furnstahl R J and Schwenk A. Prog. Part. Nucl. Phys. 65 94 (2010)

[28] Furnstahl R. J. and Hebeler K. Rep. Prog. Phys. 76, 126301(2013)

[29] D. R. Entem and R. Machleidt. Phys. Rev. C 68, 041001 (2003).

[30] S. Kvaal, Phys. Rev. C 78, 044330 (2008).

[31] G.P. Kamuntavicius, R.K. Kalinauskas, B.R. Barrett, S.Mickevicius, D. Germanas, Nucl. Phys. A 695, 191 (2001).

[32] G. Puddu.Eur. Phys. J. A 51, 14(2015).

[33] W. Lederman (Editor), Handbook of Applicable Mathemat- ics, Vol. III, Numerical Methods (John Wiley and Sons, New York, 1981) chapt. 11.

[34] G. Puddu, Eur. Phys. J. A 42, 281 (2009)

[35] Handbook of Mathematical Functions. Eds. M.Abramowitz and I.A. Stegun. Washington D.C. 1972.

[36] J.M.Yao, J.Engel, L.J.Wang,C. F. Jiao and H. Hergert. Phys. Rev. C 98, 054311 (2018).

[37] G. Audi and A.H. Wapstra. Nucl. Phys. A565, 1 (1993).

[38] H. Hergert, S. Binder, A. Calci, J. Langhammer and R. Roth. Phys.Rev.Lett. 110, 242501 (2013).

[39] R.Roth. Phys. Rev. C 79, 064324 (2009).